



A01-34447

AIAA 01-3797

Experimental/Computational Investigation of  
Electric Arc Air-Spikes in Hypersonic Flow  
with Drag Measurements

R.M. Bracken, L.N. Myrabo,  
H.T. Nagamatsu, and E.D. Meloney  
Department of Mechanical Engineering, Aeronautical  
Engineering, and Mechanics  
Rensselaer Polytechnic Institute  
Troy, NY  
And  
M.N. Shneider  
Princeton University  
Princeton, NJ

**37<sup>th</sup> AIAA/ASME/SAE/ASEE  
Joint Propulsion Conference  
8-11 July 2001 / Salt Lake City, UT**

For permission to copy or to republish, contact the copyright owner named on the first page.  
For AIAA-held copyright, write to AIAA Permissions Department,  
1801 Alexander Bell Drive, Suite 500, Reston, VA, 20191-4344.

# EXPERIMENTAL AND COMPUTATIONAL INVESTIGATION OF AN ELECTRIC ARC AIR-SPIKE IN HYPERSONIC FLOW WITH DRAG MEASUREMENTS

R.M. Bracken<sup>\*</sup>, L.N. Myrabo<sup>†</sup>, H.T. Nagamatsu<sup>‡</sup>, E.D. Meloney<sup>§</sup>  
*Department of Mechanical Engineering, Aeronautical Engineering, and Mechanics  
Rensselaer Polytechnic Institute  
Troy, New York 12180*

and  
M. N. Shneider<sup>¶</sup>  
*Princeton University  
Princeton, NJ 08544*

## ABSTRACT

The effects of an arc discharge to create an Air-Spike in a hypersonic flow are currently being studied in the Rensselaer Polytechnic Institute 24-inch Hypersonic Shock Tunnel (RPI HST), modeled computationally, and compared to existing theory. The arc is a high current car battery array-driven, 75-kilowatt peak, self-sustaining electrical discharge in a Mach 10, 260 psia stagnation pressure, and 560 K stagnation temperature flow. In this low enthalpy, "ideal gas," condition, schlieren photographs are taken of the apparatus with and without a downstream blunt body, with varying arc powers. Blunt body drag measurements are also made with both hanging and sliding models with fast-response accelerometers, with and without the arc to establish a correlation between arc power and body drag. The computational effort employs the Euler gasdynamic equations to represent a heat source in flow conditions and geometries identical to those tested in the RPI HST. These two results are then compared to early Air-Spike theoretical predictions to qualitatively validate the CFD code and gain a better perspective on the loss mechanisms involved in the experiment.

## INTRODUCTION

Among the most critical factors in the design of a hypersonic vehicle are aerodynamic drag and heating. To design for low aerodynamic drag would leave the body with sharp edges and a high fineness ratio. Heat transfer concerns would lead the design to a blunt body with a very low fineness ratio, which leads to a substantial increase in wave drag. It has been suggested by several authors (Myrabo<sup>1</sup>, 1978, Tidman<sup>2</sup>, 1990, Myrabo<sup>3</sup>, *et al.*, 1994, Head<sup>4</sup>, 1994, Seo<sup>5</sup>, 1994, Gurijanov<sup>6</sup>, *et al.*, 1996, and Covault<sup>7</sup> 1999) that both the drag and heating of a hypersonic Trans-Atmospheric Vehicle (TAV) could be greatly reduced by adding energy to the air ahead of the craft. This energy addition could be accomplished through the focusing of beamed electromagnetic radiation from a laser or microwave source. Figure 1 shows a diagram of this concept of focusing a laser beam to support the Directed-Energy Air-Spike (DEAS). Marsh<sup>8</sup>, *et al.*, (1996), have experimentally demonstrated that the strong bow shock wave normally produced by a blunt body would become a more benign conical shock wave when an electric arc torch is fired ahead of the body. Figure 2 is a schlieren photo from these tests.

<sup>\*</sup> Graduate Student, AIAA Student Member  
<sup>†</sup> Associate Professor of Engineering Physics, AIAA Senior Member  
<sup>‡</sup> Active Professor Emeritus of Aeronautical Engineering, AIAA Fellow  
<sup>§</sup> Graduate Student, AIAA Student Member  
<sup>¶</sup> Researcher, AIAA Member

Copyright ©2001 by R.M. Bracken and L.N. Myrabo.  
Published by the American Institute of Aeronautics and Astronautics, Inc, with permission.

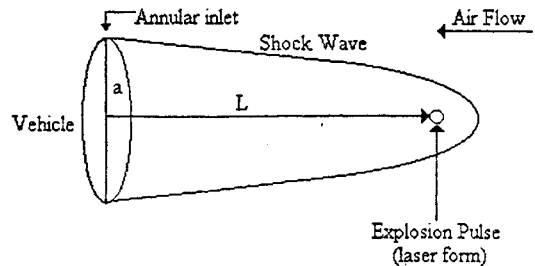
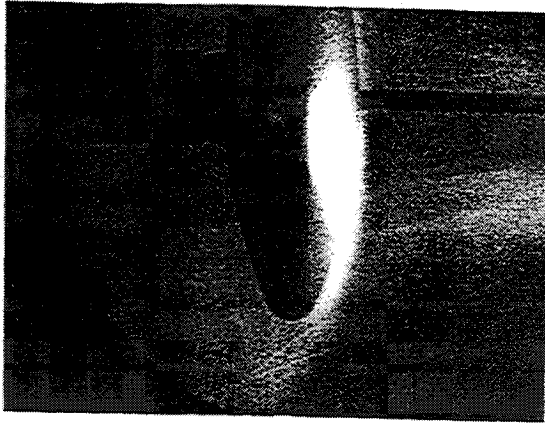


Fig. 1 Laser Supported Directed-Energy Air-Spike



**Fig. 2 Effect of the Electric Plasma Torch (35kW) on the Mach 10 Flow Over a Blunt Body**

Later, Toro<sup>9,10</sup> *et al.*, (1999), conducted additional tests using the same apparatus but fitted the blunt body model with piezoelectric pressure transducers and platinum thin-film heat transfer gages. The surface and impact (taken at the model periphery) pressure measurements indicated a decrease in aerodynamic drag; the heat transfer measurements revealed a decrease in surface heat transfer. These experiments were conducted for Mach 10 ideal gas conditions with arc torch electric powers up to 127kW. Nevertheless, these interesting results are affected by the physical presence of the plasma torch itself, which behaves as a mechanical spike (Bogdonoff<sup>11</sup> *et al.*, 1958), and provides beneficial counter airflow (Moraes<sup>12</sup> *et al.*, 1985) at the torch tip.

Most recently, a “torchless” apparatus has been used to minimize flow disturbance and mitigate the two aforementioned properties of the torch. In initial testing, a Maxwell capacitor bank was used as the power supply, providing the high power necessary to induce and sustain an electric discharge between two thin electrodes diametrically opposed and perpendicular to the hypersonic flow (Minucci<sup>13</sup> *et al.*, 2000). The present experiment, however, employs a direct current car battery array power supply to alleviate measurement difficulties incurred by the transient nature of the capacitor discharge, as well as different electrode geometries to minimize flow disturbance. The same blunt body used by Toro,<sup>6,7</sup> *et al.*, (1999) is also employed for these tests, with preliminary drag and requisite pressure transducer measurements taken.

### EXPERIMENTAL APPARATUS

The electric arc-simulated Air-Spike tests were conducted in RPI’s Hypersonic Shock Tunnel,

seen in Figure 3. The facility is capable of producing test section Mach numbers ranging from 8 to 25, stagnation temperatures and pressures of 4100 K and 1500 psi, respectively, and useful test times on the order of 4 milliseconds. The high enthalpy condition can be achieved by operating the tunnel in the equilibrium interface condition (Minucci<sup>14</sup> *et al.*, 1994), using argon as the gaseous piston (Nascimento<sup>15,16</sup> *et al.*, 1997, 1998). A more comprehensive description of the facility can be found elsewhere (Minucci<sup>17</sup> *et al.*, 1991).

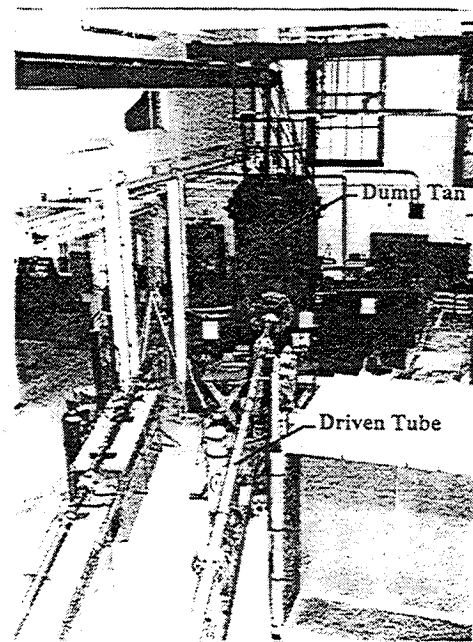


**Fig. 3 RPI HST Facility**

The RPI HST data acquisition capabilities consist of both electronic and optical measurement systems. Pressure and heat transfer measurements, made by PCB piezoelectric pressure transducers and platinum thin-film heat transfer gages, as well as any other necessary electronic measurements, are recorded utilizing Tektronix VXI and 2520 Test Lab systems. These electronic data systems are integrated and controlled by a Labview<sup>TM</sup> program.

Optical data capabilities include both natural luminosity and single-pass laser schlieren photography. A borrowed Beckman & Whitley Inc. model 350 high-speed framing camera increases our luminosity filming capabilities from a single time-integrated photograph to up to 35,000 frames per second, for a maximum of 224 pictures per test. The camera is also adaptable to a streak configuration, allowing Schlieren picture rates from 2,000 to 5,000 frames per second, employing a repetitively pulsed Oxford 20 W copper vapor laser. All flow visualization photography uses the two 9-in diameter

windows at opposite sides of the test section. Figure 4 is a schematic view of the hypersonic shock tunnel driven section end and dump tank, indicating the position of the aforementioned components.

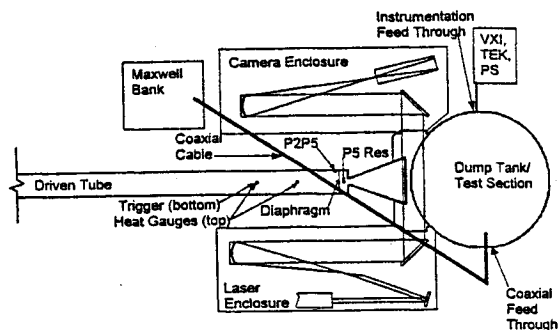


Fig. 4 HST Instrumentation Layout

Four electrical power supplies are commonly used in conjunction with experiments in the RPI HST. 1) A specially constructed 1080 V battery unit provides high voltage, low current discharges for applications requiring a low noise, moderate power direct current. 2) For low voltage, high current needs, a Miller Model SRH 333 arc welder power supply can produce 70 VDC at 600 A. As previously mentioned, the welder was used by Marsh<sup>5</sup> *et al.*, (1996) and Toro<sup>6,7</sup> *et al.*, (1999) in similar flow conditions, to produce an arc at the end of a physical spike (i.e. a plasma torch), instead of externally in the freestream, as it was employed here. 3) Experiments requiring both high voltage and current utilize a donated Maxwell capacitor bank (Figure 4). This power supply can produce 10 kV with currents up to 100 kA, for short durations. The capacitor bank has been successfully used in the past for other shock tunnel experiments (Kerl<sup>18</sup> *et al.*, 1999). 4) For moderate voltages (240 Volts) and high currents (1300 Amperes) a DC lead-acid battery array is employed.

The power supply chosen for a given experiment is connected to the apparatus in the test section employing a coaxial copper pipe-welding cable power line. A ceramic feed-through plate allows the coaxial power line to pass through the dump tank wall (Figure 5), while retaining vacuum and insulating the line from the steel wall.

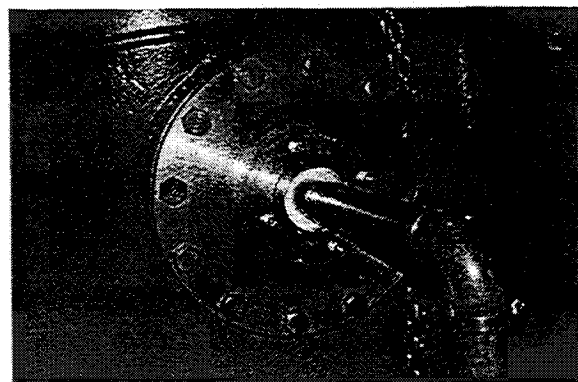


Fig. 5 Test Section Electric Feed Through

### DEAS APPARATUS

The principal apparatus used in the present experiment is a nylon ring-supported electrode structure used to create an arc in a hypersonic flow. The nylon ring serves to insulate the copper terminals from the 24-in diameter aluminum nozzle exit of the HST, as well as providing some vibration isolation. This “torchless” arc configuration was fabricated in RPI’s Central Machine Shop. To minimize disturbance of the hypersonic freestream, the thin electrodes were designed to span as much of the 24-in nozzle diameter as possible. The positioning of the electrodes is quite variable, opposable by 90° or 180°, and continuously variable in sweep.

The electrodes are 1/16-in diameter, 7-in long zirconiated-tungsten rods. This particular alloy is generally implemented in high power, alternating current arc welding. The highly brittle alloy, albeit resistant to high current, is prone to shear failure in the Mach 10 flow. Attaching low-profile steel supports behind the electrodes abated the problem.

In this phase, a car battery array supplies power to the electrodes in the freestream, a configuration that requires the two electrodes to touch, then burn back during the test. Once the arc is established, the current density of more than 300,000 Amps/in<sup>2</sup> through the electrodes easily sustains the arc, even in the presence of a hypersonic freestream (Bracken<sup>19</sup> *et al.*, 2001).

The electrical circuit diagram for connecting the power supply to the electrodes is depicted in Figure 6. The current monitor and a parallel-shunt current monitor (for voltage) allow for dynamic measurements of the electric current and voltage, respectively. Since the electrodes ablate fairly rapidly, the discharge has to be timed with the shock tunnel run. This was accomplished with the combination of a high current SCR to fire the arc and a household 20 Amp circuit breaker to end the test.

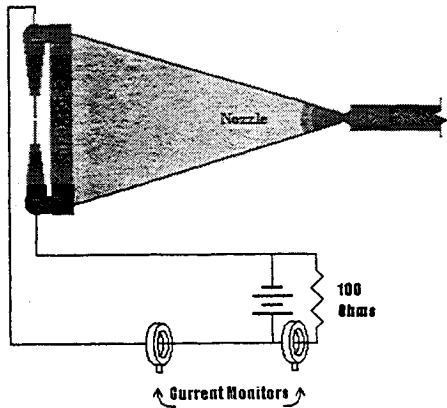


**Fig. 6 Power Supply Circuit Diagram**

A first-generation drag measurement system has been tested in the RPI HST using a blunt body fitted with a fast response PCB accelerometer and suspended by thin wire. The blunt body is able to move freely in the axial direction, allowing the use of simplified free-body equations. A depiction of the configuration is shown in Fig. 7.

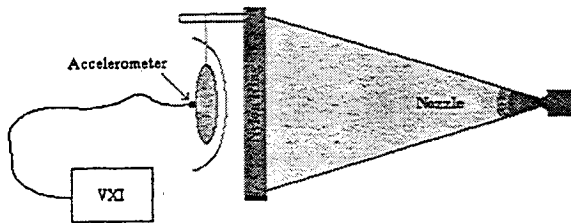


**Fig. 7 Preliminary Drag Model Configuration**

A second-generation drag model was also tested in the shock tunnel. A brass model slides in the axial direction on a tubular stainless-steel sting-mount (Fig. 8) in order to minimize post-test impacts with

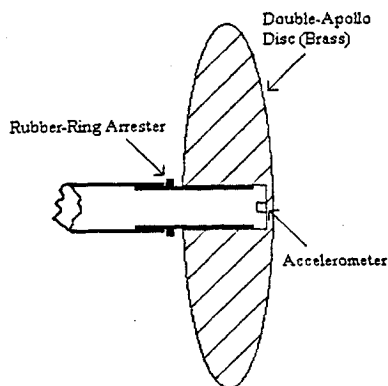


**Fig. 8 2<sup>nd</sup>-Generation Drag Model Components**

delicate instruments inside the test section. The blunt body is confined to purely axial-translational motion along a distance of approximately  $\frac{1}{4}$  inch, before being brought to rest by a foam rubber ring. Fig. 9 is a photograph of the second-generation model.

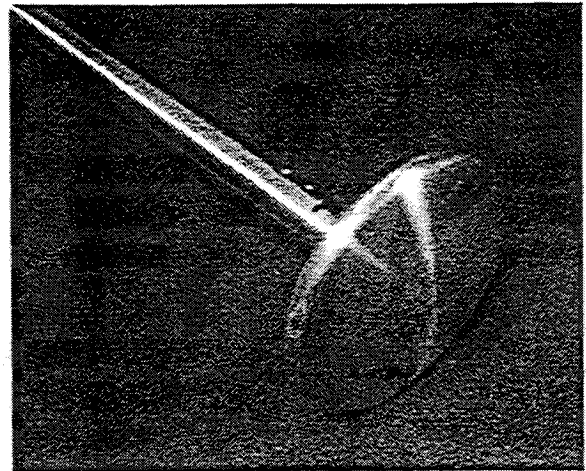


**Fig. 9 Second Generation Drag Model**

## EXPERIMENTAL RESULTS

Three major experimental phases were conducted. 1) An arc was fired in the freestream of the RPI HST. 2) A blunt was placed in the freestream. 3) An arc was discharged upstream of the blunt body. All tests presented in this paper were conducted in the RPI HST in Mach 10, low enthalpy flow with stagnation temperature and pressure of 560 K and 260 psi, respectively.

### **Arc in Freestream**

To gain a perspective on the fundamental phenomena behind the effects of an energy release in a hypersonic flow an arc is established between thin electrodes in the RPI HST. The primary diagnostics are arc power measurements and resulting shock wave shapes. Two cases were tested in Mach 10, low enthalpy flow, with arc powers of approximately 13 kW and 30 kW. The shock waves for these cases were imaged using a high-speed schlieren camera recording photographs at 4500 frames per second. A sample photograph from each test is shown in Figures 10 and 11.



Fig. 10 Mach 10 Flow with 13 kW Arc Power

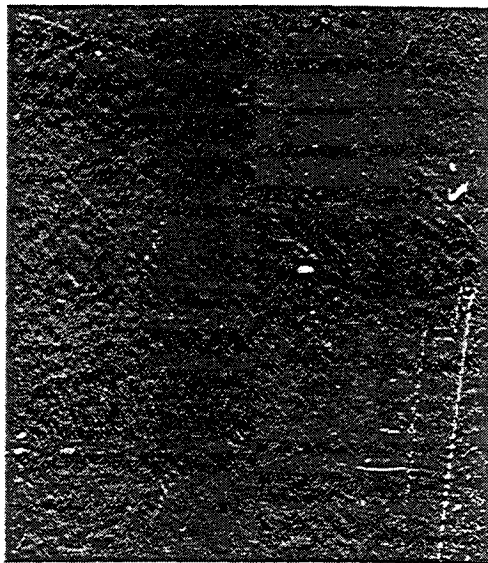


Fig. 11 Mach 10 Flow with 30 kW Arc Power

The parabolic nature of the shock wave structure is immediately obvious in Figures 10 and 11. Noting this, the shock wave from each photograph was fit with a second-order polynomial regression in order to begin to quantify its shape. Figure 12 shows parabolic fits of the same shock waves seen in Figures 10 and 11. These figures show two very notable properties of the shock wave. 1) The shock (in general) is well fit by the parabolic approximation ( $R^2$  is nearly unity). 2) The shock near and upstream of the arc is not well fit by the same parabola that fits the rest of the shock.

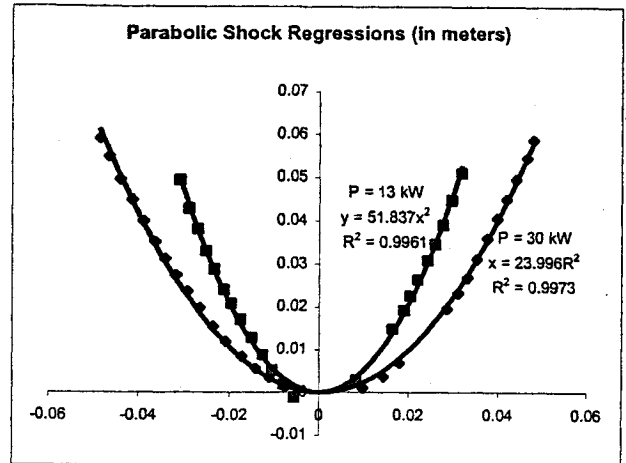


Fig. 12 Parabolic Shockwave Fits

Since voltage and current measurements are made across the entire circuit, it is clear that what is measured is not the arc power. The major resistive components of the circuit are the circuit's inherent, steady current resistance, the inductive resistance, and the dynamic arc resistance, all of which are described in the equation for voltage:

$$V = R_a i + R_c i + L_c \frac{di}{dt} \quad (1)$$

where  $V$  is the measured total circuit voltage,  $R_a$  is the arc resistance,  $R_c$  is the circuit component resistance,  $L_c$  is the circuit inductance, and  $i$  is the measured current. The inductive term becomes negligible since the circuit has a very low inductance and we are taking measurements during the "steady-state" region of the power curve shown in Figure 13.

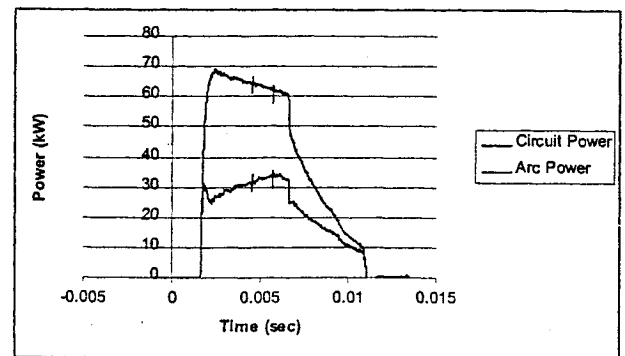


Fig. 13 Typical Circuit and Arc Power Traces

### Blunt Body in Freestream

For drag tests, the RPI HST was again run in low enthalpy, Mach 10 conditions. To fully characterize the flow and drag characteristics, pitot pressure, acceleration values, and high-speed schlieren photographs were recorded.

Blunt body acceleration traces showed very high levels of noise in the trace. To relieve the accelerometer signal of high frequency noise, a simple spreadsheet filter was used, yielding promising traces. To establish the validity of the acceleration trace, we use the simple relation,

$$D_m = m_m a \quad (2)$$

where  $D_m$  is the drag on the model,  $m_m$  is the model mass, and  $a$  is the measured acceleration. Shown in Figure 14, this trace, shows very good qualitative agreement when compared to the measured pitot pressure trace (Figure 15).

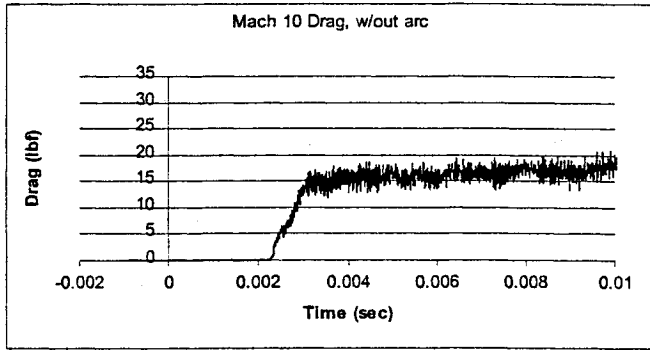


Fig. 14 Drag Trace With No Arc

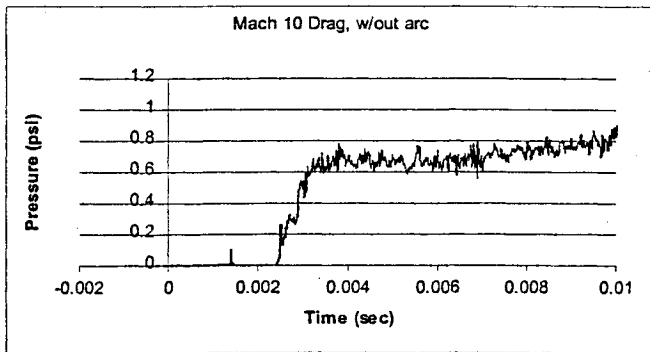


Fig. 15 Pitot Pressure Trace

To compare measured drag coefficients with theoretical values, we begin with the familiar drag equation,

$$D = qSC_D \quad (3)$$

where

$$q = \frac{1}{2} \rho_1 v_1^2 = \frac{\gamma p_1}{2} M_1^2 \quad (4)$$

is the dynamic pressure,  $S$  is the frontal area of the model, and  $C_D$  is the coefficient of drag. To determine the freestream total pressure, two ideal gas normal shock relations were utilized:

$$\frac{P_{t2}}{P_{t1}} = \left[ \frac{(\gamma + 1)M_1^2}{(\gamma - 1)M_1^2 + 2} \right]^{\frac{\gamma}{\gamma - 1}} \left[ \frac{(\gamma + 1)}{2\gamma M_1^2 - (\gamma - 1)} \right]^{\frac{1}{\gamma - 1}} \quad (5)$$

$$\frac{P_{t2}}{P_1} = \left[ \frac{(\gamma + 1)M_1^2}{2} \right]^{\frac{\gamma}{\gamma - 1}} \left[ \frac{(\gamma + 1)}{2\gamma M_1^2 - (\gamma - 1)} \right]^{\frac{1}{\gamma - 1}} \quad (6)$$

These equations are used to relate the measured total pressure behind a normal shock to the freestream conditions upstream of the blunt body. The experimental drag coefficient of the blunt body can be expressed as

$$C_D = \frac{D_m}{qS} = \frac{D_m}{\frac{\gamma p_1 M_1^2}{2} S} \quad (7)$$

and substituting equation (5) for the static pressure, noting that  $\gamma = 1.4$ ,

$$C_D = \frac{2D_m}{\gamma P_{t2} S M_1^2} \left[ \left( \frac{6M_1^2}{5} \right)^{\frac{7}{2}} \left( \frac{6}{7M_1^2 - 1} \right)^{\frac{5}{2}} \right] \quad (8)$$

Using this equation we calculate an experimental dynamic drag coefficient with respect to the freestream conditions. The drag coefficient shown in Fig. 16 agrees very well with modified Newton theoretical predictions and historical experimental data of a flat disc in high Mach number flow (Summerfield<sup>20</sup>, 1986) and inspires confidence in the accuracy of the accelerometer drag system.

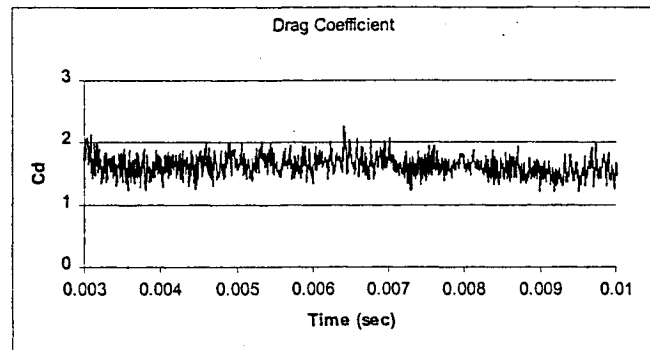


Fig. 16 Blunt Body Drag Coefficient Trace

The second-generation drag model produced interesting results though complicated by the existence of inconsistent bearing surface drag. At the very small time scales in which the drag model acquires data the friction is no longer constant but random, noisy, and very much larger in peak amplitude than the measured average.

Though clearly not useful for powered runs where drag will be changing dynamically where it would be difficult to determine when the model is sticking and when it is sliding, the model did serve to corroborate the drag coefficient values obtained in the earlier (hanging) tests. Figure 17 is an overlay of the drag forces obtained in the sliding and hanging models showing that while freely sliding the second-generation model agrees very well with the hanging model. This is especially encouraging since the model is made of brass as opposed to aluminum, so has much higher mass and therefore lower acceleration values for the same input force.

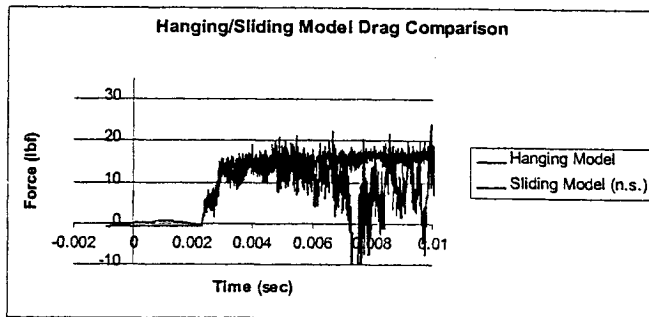


Fig. 17 Hanging/Sliding Drag Measurements

#### Blunt Body in Arc Wake

The accelerometer-instrumented drag model was also tested within the wake of the arc. Since the raw acceleration trace was again very noisy, the smoothing routine was applied which yielded the trace shown against the no-arc case in Figure 18.

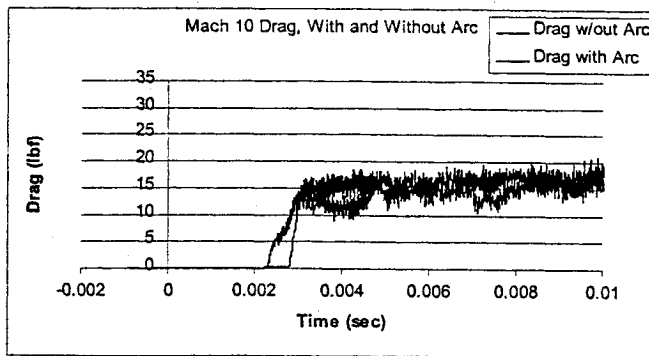


Fig. 18 Drag Traces With and Without Arc

The preliminary nature of these results precludes detailed quantitative analysis. It is clear, however, that the model experienced less drag throughout much of the test time with the arc than without. By referring to Figure 19 a generally inverse relationship can be seen between the drag and the arc power. Figures 20 and 21 show the blunt body shock structure without and with the upstream arc, respectively.

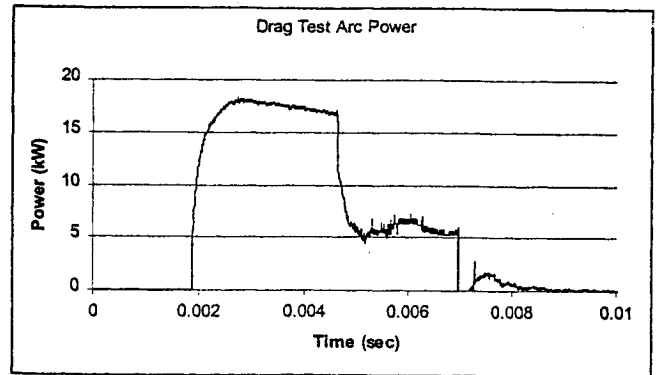


Fig. 19 Arc Power for Drag Test, Run 27

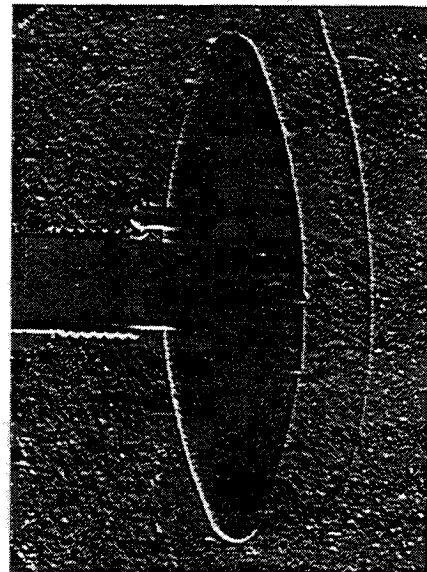


Fig. 20 Blunt Body in Mach 10 Flow, No Arc

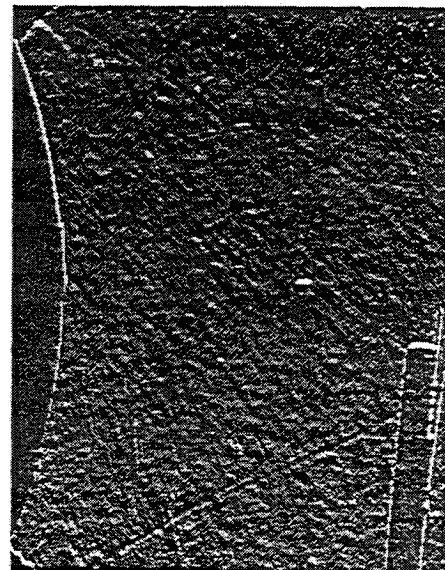


Fig. 21 Blunt Body in Mach 10 Flow, 30 kW Arc

## COMPUTATIONAL RESULTS

The Air-Spike was also modeled using the full set of Euler gasdynamic equations in cylindrical coordinates,

$$\frac{\partial}{\partial t} U + \frac{\partial}{\partial r} R + \frac{\partial}{\partial z} Z = H, \quad (9-13)$$

$$U = \begin{pmatrix} \rho \\ \rho u \\ \rho w \\ e \end{pmatrix}, \quad R = \begin{pmatrix} \rho u \\ \rho u^2 + p \\ \rho w u \\ (e+p)u \end{pmatrix}, \quad Z = \begin{pmatrix} \rho w \\ \rho w u \\ \rho w^2 + p \\ (e+p)w \end{pmatrix}, \quad H = -\frac{1}{r} \begin{pmatrix} \rho u \\ \rho u^2 \\ \rho w u \\ (e+p)u \end{pmatrix} + \begin{pmatrix} 0 \\ 0 \\ 0 \\ Q \end{pmatrix}$$

$$e = \rho \left[ \varepsilon + (u^2 + w^2)/2 \right], \quad (14)$$

where  $\rho$  and  $p$  denote the gas density and pressure, respectively,  $u, w$  are the  $r$  and  $z$  velocity components,  $e$  is the total energy of gas per unit volume,  $\varepsilon$  is the internal energy per unit mass, and  $Q(r, z)$  is the power density of the source of energy release ( $W/cm^3$ ). The Gaussian distribution:

$$Q(r, z) = \frac{P}{\pi^{3/2} \Lambda^3} \exp \left[ -\frac{r^2 + (z - z_q)^2}{\Lambda^2} \right], \quad (15)$$

is assumed for  $Q(r, z)$ , where  $P$  is the total power absorbed in the flow, and  $z_q$  is the coordinate of the heat source center. The equation of state for ideal gas  $p = (\gamma - 1)\rho\varepsilon$ , was used to close the system of gasdynamic equations. The temperature dependence of  $\gamma$  was included for the instantaneous distribution of internal energy  $\varepsilon(r, z) = p/(\gamma - 1)\rho$  derived in calculations. The gas temperature distribution  $T(r, z) \equiv T(\varepsilon, \rho)$  was determined by quadratic interpolation using the tables of thermodynamic functions for hot air Kuznetsov *et al.*, 1965<sup>21</sup> thus enabling one to select the space distribution of  $\gamma(T)$  for the next time step.

The calculation for cases with and without blunt body in hypersonic stream was performed until complete time relaxation of all parameters was attained, using the 'rippling through' method in the McCormack scheme of the second order of accuracy (Anderson<sup>22</sup> *et al.*, 1984). Since computations were done on a rectangular grid, the physical coordinates  $(r, z)$  were transformed into  $(\bar{r}, \bar{z})$ :

$$\bar{r} = r / r_{\max}$$

$$\bar{z} = \frac{z - z_b(r)}{z_{\max} - z_b(r)}, \quad \bar{z}, \bar{r} \in [0, 1],$$

where  $z_b(r)$  is the blunt body surface. The flow velocity component normal to the blunt body surface was assumed to be zero.

The calculations were performed for the incident flow parameters corresponding to the RPI HST experimental conditions: Mach number of the incident flow,  $M=10.1$ , static pressure  $p_\infty = 5.6 \cdot 10^{-3}$  psi = 38.6 Pa, static temperature,  $T_\infty = 37.7$  K, and sound velocity of unperturbed flow,  $c_\infty \approx 123.1$  m/s. The control of calculative accuracy in the steady state regime requires an error of less than 0.5 %:

$$2\pi \left\{ \int_0^{r_{\max}} r [(e+p)w]_{z_{in}} dr - \int_{r_{b,\max}}^{r_{\max}} r [(e+p)w]_{z_{out}} dr \right\} / P \rightarrow 1$$

These computations have lead to some very interesting results. Figures 22 and 23 show the results of this code for an energy release without and with a downstream blunt body.

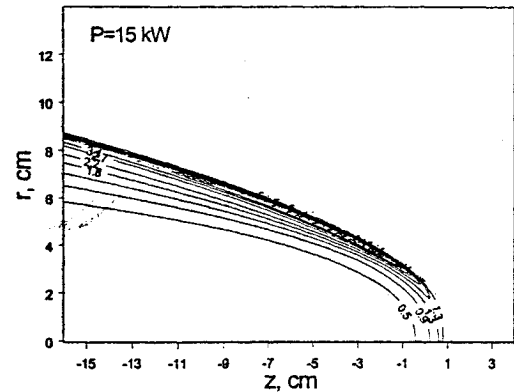


Fig. 22 Mach 10 Freestream with 15 kW Source (No Downstream Blunt Body)

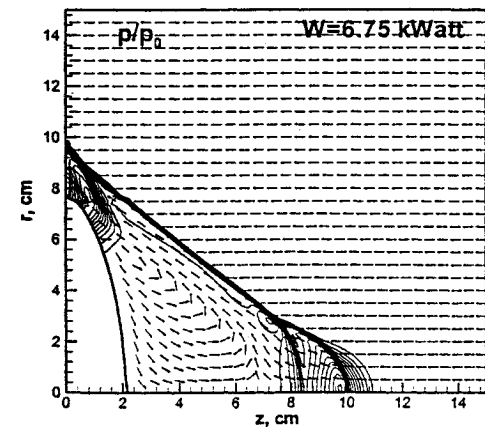


Fig. 23 Mach 10 Flow with 6.75 kW Source upstream of Blunt Body

### COMPARISONS OF THEORY, COMPUTATIONS, AND EXPERIMENT

Myrabo and Raizer<sup>3</sup>, 1994, used the law of self-similar propagation of a strong shock induced by a blast wave to obtain the expression:

$$R = \alpha \left( \frac{P}{\rho v^3} \right)^{1/4} x^{1/2} \quad (16)$$

where

$$\alpha = \left[ \frac{4(\gamma + 1)(\gamma^2 - 1)}{\pi(3\gamma - 1)} \right]^{1/4} = .937 \text{ for } \gamma = 4/3 ,$$

$R$  is the radius of the shock wave at  $x$ , the distance aft of the shock leading edge,  $P$  is arc power,  $\rho$  is air density, and  $v$  is air velocity. For steady state conditions, this describes the parabola,  $x = cR^2$ , when:

$$c = \frac{1}{\alpha^2} \left( \frac{P}{\rho v^3} \right)^{-1/2} \quad (17)$$

This parabolic coefficient is used as a means of comparison between the power and resulting shock wave shapes by rearranging the above equation in terms of power:

$$P = \frac{\rho v^3}{(c\alpha)^2} \quad (18)$$

The power predicted by this equation serves as a medium by which to compare the theoretical predictions of Myrabo and Raizer (Ref. 3), the numerical predictions presented in this paper, and experimentally obtained results. The shock wave produced by an arc of 30 kW is predicted by the above equation to require 13 kW, while the numerical analysis shows approximately 15 kW. The error, while high, is not unexpected. In fact, since radiative and ablative losses have been postulated at about 50%, this would seem to agree very well. Most important to our present objectives is the fact that the theory very accurately predicts the shape of the shock wave. Nevertheless, better quantitative agreement will not be possible until the effect of these major loss mechanisms are addressed.

Other (more qualitative) properties of the experiment are being well characterized by the computational analysis. The shape of the split shock wave resulting from power addition to the flow ahead of the blunt body is apparent in the CFD results, as can be seen in Fig. 21 and Fig. 23. This secondary shock is indicative of a recirculation zone between the blunt body and power source to provide incoming flow with a second turn angle. The analysis shown in

Figure 23, does, however need further refinement in two major areas: 1) near the heat source where the shock is not well defined. When the size of the heat source is reduced to the point where it does not extend beyond the fore shock the code becomes unstable. Because of this, the Gaussian shaped heat distribution has to be enlarged to such a degree that the flow is gradually heated and turned, eliminating the fore shock in the analysis. Using a much tighter grid in the area of the heat source, which was not ideal for the purposes of this paper, but will be considered in the future, will solve this problem. 2) Near the axis a shock should not occur as it does in the computations. The heat released ahead of the (erroneous) secondary shock seen in Fig. 23 should be enough to render the flow in the proximity of the axis subsonic and preclude the existence of any further shock waves on the axis of the model.

### SUMMARY AND FUTURE WORK

- ◆ An arc is established in Mach 10 flow between the two Tungsten electrodes, driven by an array of high current lead-acid batteries at powers up to 75 kW.
- ◆ High-speed schlieren photography is used to image the effect of the arc on a Mach 10 flow with no blunt body, showing a parabolic shock with a significant standoff distance from the arc center.
- ◆ The Air-Spike shock wave resulting from an arc with no downstream blunt body is well fit by the parabolic blast wave equation from Ref. 2.
- ◆ A free-hanging blunt body is instrumented with an accelerometer and aerodynamic drag is measured.
- ◆ Measured drag coefficient agrees well with theory and historical data.
- ◆ Preliminary drag measurements show a reduction in drag on the blunt body when an arc is fired upstream.
- ◆ Numerical computations are made using the RPI HST Air-Spike setup and Euler's gasdynamic equations to provide insight into the fundamental loss mechanisms and to seek preliminary validation of the CFD code.
- ◆ The next-generation model will return to a hanging system but will include provisions for off-axis accelerometers to measure side forces and moments.
- ◆ Future tests will be conducted to determine maximum drag reduction efficiencies with respect to input power and upstream distance.